Elastoplastic Modelling of Hydro-mechanical Behaviour of Unsaturated Soils

J. R. Zhang[1], D. A. Sun[2] and W. J. Sun[3]
[1] Henan Province Key Laboratory of Rock and Soil Mechanics and Structural Engineering,
North China University of Water Resources and Electric Power, Zhengzhou, China
[2,3] Department of Civil Engineering, Shanghai University, Shanghai, China.
E-mail: sundean@shu.edu.cn

ABSTRACT: The development of constitutive models for unsaturated soils is briefly reviewed, and the state-of-the-art of elastoplastic constitutive models for unsaturated soils is summarized. This paper introduces an elastoplastic model that couples hydraulic and mechanical behaviour for unsaturated non-expansive and expansive soils. The two coupled elastoplastic constitutive models are illustrated with laboratory tests to show their application and performance. Hydraulic hysteresis in the soil-water characteristic is modeled as an elastoplastic process with the elastic region of the degree of saturation. The effect of change in degree of saturation on the stress-strain-strength behaviour and the effect of change in void ratio on the soil-water characteristics are taken into consideration in the model in addition to the effect of suction on the hydraulic and mechanical behaviour.

KEYWORDS: Unsaturated soil, Elastoplastic model, Stress-strain relation, Soil-water characteristic, Coupling

1. INTRODUCTION

Following an comprehensive analysis of unsaturated non-expansive and expansive soils behavior (Alonso et al. 1987), an elastoplastic constitutive model for unsaturated non-expansive soils, known as the Barcelona Basic Model (BBM), was formulated by Alonso and co-workers (Alonso et al. 1990). Since then, several constitutive models based on this fundamental model have been developed. At the beginning, as in the BBM, only the relationship between stress, suction and strain was addressed (Kogho et al. 1993, Wheeler and Sivakumar 1995, Sun et al. 2000, among others). Almost all constitutive models for unsaturated soils used the concept of two independent stress variables that was developed initially by Coleman (1962) and later established by Fredlund and Morgenstern (1977). As summarized by Gens *et al*. (2006), the two stress variables used in most existing models can be expressed as

$$\left(\sigma_{ij} - u_a \delta_{ij}\right) + \mu_1(s,...)\delta_{ij};\ \mu_2(s,...) \tag{1}$$

where μ_1 and μ_2 are functions of either suction *s* (here it is limited to matric suction) or suction and other variables.

In order to account for the hysteresis phenomenon observed in unsaturated soils when subjected to wetting-drying cycles, a new variable related to water quantity (specific volume of water or degree of saturation) was later introduced (Wheeler *et al*. 2003, Sheng *et a*l. 2004, Sun *et al*. 2007a, 2007b and 2007c, among others). This necessitates the incorporation of the suction-water saturation relationship into the stress-suction-strain relationship mentioned above. The existing elastoplastic constitutive models for unsaturated soils are almost exclusively based on experimental studies of compacted specimens, and cannot describe well the hydro-mechanical behaviour of pre-consolidated slurry clays.

A new approach was proposed by Sheng et al. (2008) for unsaturated soils. The fundamental idea is that the yield stress and shear strength functions are derived from a continuous and smooth volume change equation. Consequently all these functions are continuous and smooth over both positive and negative pore water pressures. Indeed, the load-collapse function recovers the apparent tensile strength function if the pre-consolidation stress is set to zero. The model seems to be able to predict for both air-dried samples from slurry and compacted samples. Comparisons made between model simulations and experimental results show that it is a quite promising approach.

The above models can reproduce most basic mechanical response of non-expansive unsaturated soils including collapse. However, it cannot predict the mechanical behaviour of unsaturated expansive soils. Gens and Alonso (1992) presented a framework for describing the mechanical behaviour of unsaturated expansive soils. Alonso et al. (1999) presented the Barcelona Expansive Model (BExM) in which the deformations of two level structures (microstructure and macrostructure) were considered. The mechanical behaviour of the macrostructure follows the BBM, and that of the microstructure is adopted from the framework proposed by Gens & Alonso (1992). The BExM is complicated and the micro parameters and the coupling function from micro-structural strain to macro-structural strain are difficult to be determined, and the models can only predict the stress-strain behaviour without incorporating the soil-water characteristics.

This paper presents two examples of constitutive modeling of hydro-mechanical behaviour of unsaturated non-expansive and expansive soils under isothermal conditions (Sun *et al*. 2007c, Sun and Sun 2012). It does not pretend to be a state-of-the-art report on this topic and the main objective is to show, through two constitutive models that the authors have elaborated and published in cooperation with their co-workers, how to extend a BBM-based elastoplastic model to a more complex case of hydro-mechanical loading on non-expansive and expansive soils.

2. HYDRO-MECHANICAL MODEL FOR NON-EXPANSIVE SOILS

2.1 Soil-water characteristic

It is well known that there are many factors affecting the soil-water characteristic curve (SWCC) such as the mineralogical composition, pore structure including pore size and its distribution, stress state, stress-history and temperature, etc. For a given soil and temperature, the pore structure, stress-history and stress state are main factors affecting the SWCC when the soil is subjected to changes in stress and suction. Therefore, the question is: is it necessary to take all factors into consideration in modelling the SWCC? To answer this question, let us examine some experimental data.

Figure 1 shows the measured suction plotted against the degree of saturation in wetting from the suction of 147 kPa to 0 kPa at different stress states, which are an isotropic net stress of 196 kPa, triaxial compression and extension stresses with the net principal stress ratio of 1.5 and mean net stress of 196 kPa, respectively (Sun *et al*. 2007d). The latter two stress states were applied respectively for different specimens. The specimens were compacted using a clayey silt called Pearl clay with the initial water content of about 26% and initial suction of 110 kPa. Pearl clay has a liquid limit of 43% and a plasticity index of 17.5 and is composed of 26% clay fraction (< 2 μm) and about 74% silt fraction. The clay mineralogy compositions,

determined using the X-ray diffraction test, are quartz, pyrophyllite, and kaolinite in the dominant order. Experimental data in Figures 2 to 4 and 7 to 13 are also obtained using the same soil. In Figure 1, e_0 is the initial void ratio after compaction and e_b is the void ratio just before the wetting and e_{ba} is the average value of e_b for all specimens, Comp and Ext denote triaxial compression and extension, respectively, and R is the net principal stress ratio (σ_1/σ_3). It can be seen from Figure 1 that the SWCCs are almost the same for soil specimens with a similar dry density (void ratio) in wetting although the stress states are different. This indicates that the relationship between the suction and degree of saturation in wetting is rather dependent upon the pore structure, which is simply identified by void ratio, rather than the stress state under which the suction change takes place. Similar observations are found in Nuth and Laloui (2008) and Salager et al. (2010), etc. Therefore, when we develop a mathematical model for the SWCC, the stress variables are unnecessary, but the void ratio is needed to be considered.

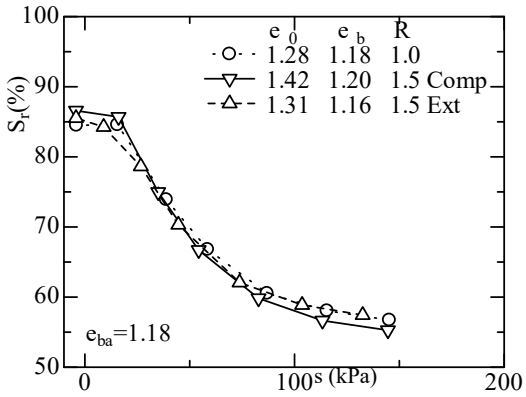

Figure 1 Wetting SWCC at different stress state with mean net stress of 196 kPa (after Sun *et al*. 2007d)

Figure 2 shows the SWCCs for two unsaturated compacted specimens A and B with different initial void ratios, obtained from the wetting tests under the same constant isotropic net stress of 20 kPa. It can be seen that when the void ratio decreases, the curve moves to the right, which means that the air-entry value increases. The micro-mechanism can be explained from the results of the mercury intrusion porosimetry (MIP) tests, as shown in Figure 3. The same soil (Pearl clay) with the same water content was compacted with different initial void ratios of 1.15 and 1.35. There are two peak pore-size distributions for compacted specimens. Although the small pore-size distributions are almost unchanged for different void ratios, low void ratio results in a decrease in the large size pore (inter-aggregate pore), which leads to an increase in the air-entry value.

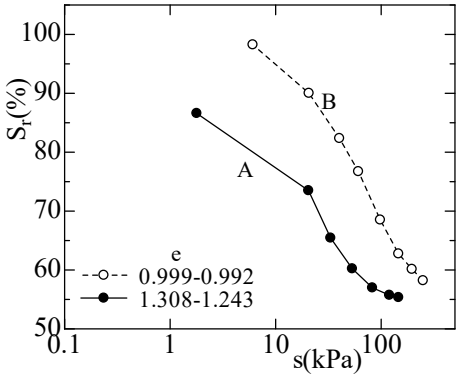

Figure 2 Wetting SWCCs at different void ratios under constant net stress of 20 kPa (after Sun *et al*. 2007a)

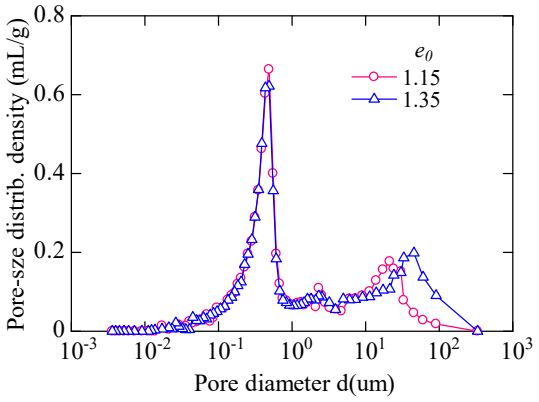

Figure 3 Pore-size distributions of compacted Pearl clay specimens with different void ratios from MIP tests

Figure 4 shows the measured relationship between degree of saturation and void ratio from triaxial tests and the corresponding stress paths during isotropic compression loading and/or triaxial shear loading under a constant suction of 147 kPa. The specimens tested were compacted at different initial void ratios and different initial degrees of saturation. It can be observed that, even under the same imposed suction (147 kPa), the degree of saturation increased when the unsaturated soil specimens were compressed. Furthermore, even under different stress paths, the measured relationship between the degree of saturation and void ratio for the specimens with different void ratios are very similar, and can be considered to be linear, as shown in Figure 4(a).

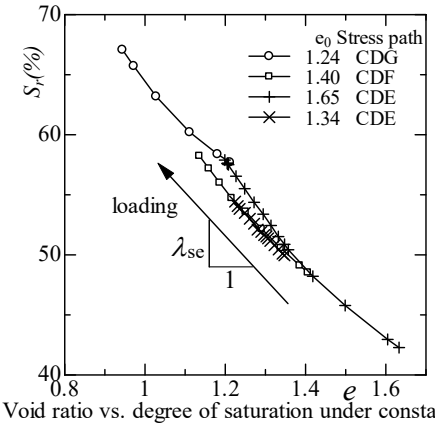

(a) Void ratio vs. degree of saturation under constant suction

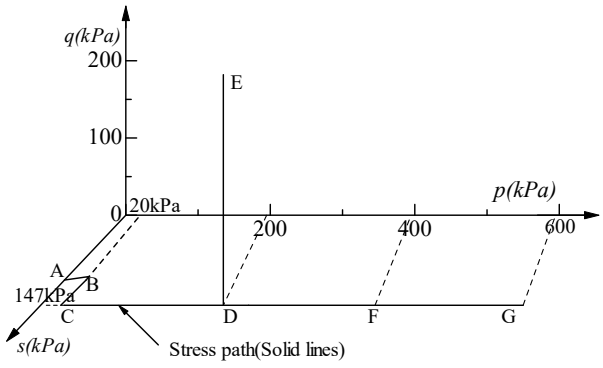

(b) Imposed stress/suction path

Figure 4 Void ratio versus degree of saturation under constant suction of 147 kPa (after Sun *et al*. 2007c)

From Figures 1, 2 and 4, it can be concluded that the SWCCs of unsaturated compacted clays depend not only on the wetting process (or drying process), but also on the void ratio (dry density), and indirectly depends on the stress state or stress history experienced. That is to say, the stress state shows insignificant effect. Therefore modeling the SWCC only needs to consider the void ratio, rather than the stress state or the stress-history. Figure 5 shows a very simple model applicable to the stress path and/or suction path for the SWCC. The main drying and wetting curves have a gradient λ_{sr} and the scanning curves have a gradient κ_s. That is to say, the changes in degree of saturation along the scanning curve and the main drying and wetting curves are expressed respectively by:

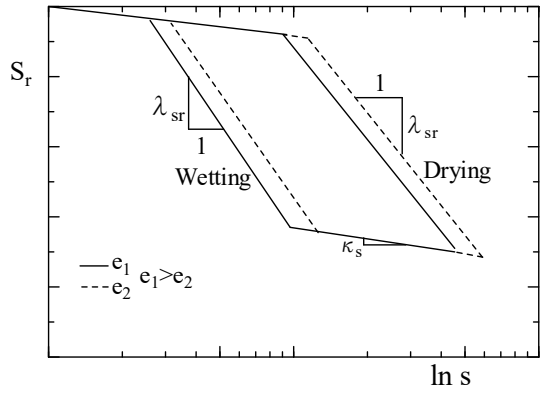

Figure 5 Modeling of SWCCs with different densities

$$\mathrm{d}S_r = -\lambda_{se}\,\mathrm{d}e - \beta\frac{\mathrm{d}s}{s} \tag{2}$$

where λ_{se} is a slope of the S_r-e curve obtained under constant suction larger than the air-entry value, and it can be determined by results of compression and/or shear tests on unsaturated soils under constant suctions, as shown in Figure 4(a), and

$$\beta = \begin{cases} \kappa_s & \text{for scanning curve} \\ \lambda_{sr} & \text{for main drying/wetting curve} \end{cases} \tag{3}$$

2.2 Stress-state variable for unsaturated soil

To identify the hydraulic and mechanical behaviour of unsaturated soils properly, the stress-state variables employed in the model are the 'average skeleton stress' tensor σ'_{ij} and the suction s, and the strain-state variables are the soil skeleton strain tensor ε_{ij} and the degree of saturation S_r. The tensor σ'_{ij} is defined by:

$$\sigma'_{ij} = \sigma_{ij} - u_a\delta_{ij} + S_r s\,\delta_{ij} \tag{4}$$

where σ_{ij} is the total stress tensor, S_r the saturation degree, u_a the pore-air pressure, and δ_{ij} the Kronecker delta. Eq. (4) is similar to the effective stress by Bishop and Blight (1963), with S_r taking the place of the weighting factor χ. The 'average skeleton stress' and the suction are not independent variables, but their work-conjugate strains (soil skeleton strains and the degree of saturation) are independent variables (Sheng et al. 2004). The 'average skeleton stress' and suction variables adopted allow a general form of hydraulic behaviour to be represented, and a smooth transition from saturated state to unsaturated state.

2.3 Formulation for isotropic stress states

Using the 'average skeleton stress' instead of net stress, a similar form of the load-collapse (LC) yield curve as in the BBM is adopted in Eq. (5), which can describe the collapse deformation due to wetting.

$$p'_y = p'_n\left(\frac{p_{0y}}{p'_n}\right)^{\frac{\lambda(0)-\kappa}{\lambda(s)-\kappa}} \tag{5}$$

where p_{0y} and p'_y are the 'average skeleton stress' yield stresses for saturated soil and unsaturated soil, respectively (see Figure 6); p'_n is an isotropic stress where unsaturated compression lines merge into saturated compression line; κ is a swelling index in the e-ln p' graph for both unsaturated and saturated soils; $\lambda(0)$ and $\lambda(s)$ are, respectively, the slopes of the normal compression lines of saturated soil and unsaturated soil in the e-ln p' graph. The $\lambda(s)$ varies with suction as follows:

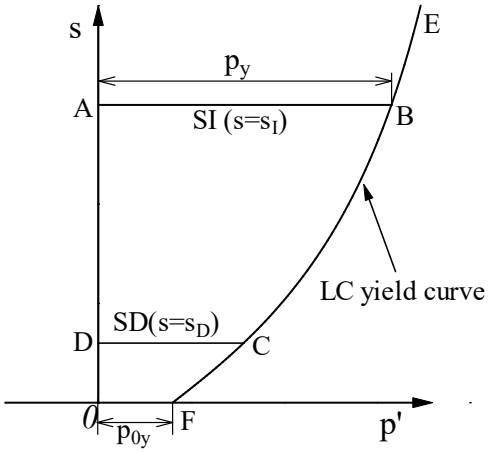

Figure 6 LC yield curve, SI and SD yield curves for isotropic stress

$$\lambda(s) = \lambda(0) + \frac{\lambda_s s}{p_a + s} \tag{6}$$

where λ_s is a soil parameter.

From Eq. (5) we have

$$dp'_y = \frac{\partial p'_y}{\partial p_{0y}}dp_{0y} + \frac{\partial p'_y}{\partial s}ds \tag{7}$$

where,

$$\frac{\partial p'_y}{\partial p_{0y}} = \frac{\lambda(0)-\kappa}{\lambda(s)-\kappa}\left(\frac{p_{0y}}{p'_n}\right)^{\frac{\lambda(0)-\lambda(s)}{\lambda(s)-\kappa}} \tag{8}$$

$$\frac{\partial p'_y}{\partial s} = \frac{\lambda_s p'_y p_a\left(\lambda(0)-\kappa\right)}{\left(\lambda(s)-\kappa\right)^2\left(p_a+s\right)^2}\ln\left(\frac{p'_n}{p_{0y}}\right) \tag{9}$$

When the stress state is inside the LC yield curve, the elastic volumetric strain increment is given by:

$$d\varepsilon_v^e = \frac{\kappa dp'}{(1+e)p'} \tag{10}$$

When the stress state is on the LC yield curve, the plastic volumetric strain increment is given by:

$$d\varepsilon_{\mathrm{v}}^{\mathrm{p}} = \frac{(\lambda(0)-\kappa)dp_{0\mathrm{y}}}{(1+e)p_{0\mathrm{y}}} \tag{11}$$

Or, from Eqs (7) and (11):

$$d\varepsilon_{\mathrm{v}}^{\mathrm{p}} = \frac{\lambda(0)-\kappa}{(1+e)p_{0\mathrm{y}}}(dp'_{\mathrm{y}} - \frac{\partial p'_{y}}{\partial s}ds) / \frac{\partial p'_{y}}{\partial p_{0\mathrm{y}}} \tag{12}$$

In addition to the LC yield curve, two more yield curves are needed to model hydraulic hysteresis as an elastoplastic process, as shown in Figure 6. The soil-water characteristic shown in Figure 4 is represented by a suction increase (SI) yield curve and a suction decrease (SD) yield curve in the p'-s graph. When the suction changes during a drying ($s \geq s_I$) or wetting ($s \leq s_D$) process, the degree of saturation increment is given by Eq. (3); otherwise, the degree of saturation increment is given by Eq. (2). Therefore, according to the relation between the stress state (p' and s) and the yield curves (LC, SI, and SD), different equations are involved in calculating the strains and the degree of saturation. When $dp_{0\mathrm{y}} > 0$ and $s > s_I$ or $s < s_D$, the volumetric strains and the degree of saturation are calculated by Eqs (10), (11), and (2). When $dp_{0\mathrm{y}} > 0$ and $s_D \leq s \leq s_I$, they are calculated by Eqs (10), (11), and (2). When $dp_{0\mathrm{y}} = 0$, and $s > s_I$ or $s < s_D$, the volumetric strain and the degree of saturation are calculated by Eqs (10) and (2). When $dp_{0\mathrm{y}} = 0$ and $s_D \leq s \leq s_I$, they are calculated by Eqs (10) and (2).

2.4 Formulation for axisymmetric stress states

The Modified Cam-clay model with elliptic yield curve has been extensively used for saturated soils, and has given reasonably good predictions for clayey soils. The elliptic yield curve and elliptic plastic potential are adopted because it is simple and all its parameters have clear physical meanings. Assuming an associated flow rule, the yield function (f) and the plastic potential function (g) are proposed to have the following form:

$$f = g = q^2 + M^2 p'(p' - p'_{\mathrm{y}}) = 0 \tag{13}$$

where p' and q' are mean value of 'average skeleton stress' and deviatoric stress, respectively, and M is the stress ratio at critical state.

The associated flow rule is applied in the 'average skeleton stress' space; that is:

$$d\varepsilon_{ij}^{\mathrm{p}} = \Lambda \frac{\partial f}{\partial \sigma'_{ij}} \tag{14}$$

where the proportionality constant Λ can be determined from the consistency condition. Eq. (13) can be rewritten as $f = f(p', q, p'_{\mathrm{y}}) = 0$, leading to:

$$df = \frac{\partial f}{\partial p'}dp' + \frac{\partial f}{\partial q}dq + \frac{\partial f}{\partial p'_{\mathrm{y}}}dp'_{\mathrm{y}} = 0 \tag{15}$$

Substituting Eq. (7) into Eq. (15) gives:

$$df = \frac{\partial f}{\partial p'}dp' + \frac{\partial f}{\partial q}dq + \frac{\partial f}{\partial p'_{\mathrm{y}}}\frac{\partial p'_{\mathrm{y}}}{\partial p_{0\mathrm{y}}}dp_{0\mathrm{y}} + \frac{\partial f}{\partial p'_{\mathrm{y}}}\frac{\partial p'_{\mathrm{y}}}{\partial s}ds = 0 \tag{16}$$

where the isotropic yielding stress p_{oy} for saturated soil is related to the volumetric strain $\varepsilon_{\mathrm{v}}^{\mathrm{p}}$ and is the same as that used in the common Cam-clay model. Because the plastic volumetric strain $\varepsilon_{\mathrm{v}}^{\mathrm{p}}$ is a hardening variable in the present model, the volumetric plastic strains $d\varepsilon_{\mathrm{v}}^{\mathrm{p}}$ caused by $dp_{0\mathrm{y}}$ in a saturated soil are the same as those in an unsaturated soil which are caused by dp'_{y} and/or ds. From Eqs (11) and (14), the following expression is obtained:

$$dp_{0\mathrm{y}} = \frac{1+e}{\lambda(0)-\kappa}p_{0\mathrm{y}}d\varepsilon_{\mathrm{v}}^{\mathrm{p}} = \frac{1+e}{\lambda(0)-\kappa}p_{0\mathrm{y}}\Lambda\frac{\partial f}{\partial p'} \tag{17}$$

Substituting Eq. (17) into Eq. (16) and solving for Λ gives:

$$\Lambda = -\frac{\frac{\partial f}{\partial p'}dp' + \frac{\partial f}{\partial q}dq + \frac{\partial f}{\partial p'_{\mathrm{y}}}\frac{\partial p'_{\mathrm{y}}}{\partial s}ds}{\frac{\partial f}{\partial p'_{\mathrm{y}}}\frac{\partial p'_{\mathrm{y}}}{\partial p_{0\mathrm{y}}}p_{0\mathrm{y}}\frac{1+e}{\lambda(0)-\kappa}\frac{\partial f}{\partial p'}} \tag{18}$$

Using Eqs (14) and (18), the plastic strain increments caused by the increment in the 'average skeleton stress' and/or the decrement in suction can be calculated.

This model has been extended to a hydro-mechanical model in three-dimensional stresses (Sun *et al*. 2007a) and a density-dependent hydro-mechanical model for unsaturated compacted soils (Sun *et al*. 2007b).

In the above constitutive model for unsaturated soils, the strain and degree of saturation are calculated from the known net stress and suction paths or the average skeleton stress and suction path. For the loading under undrained conditions or constant gravimetric water contents, the suction is not known for unsaturated soils. Our model can predict the suction and thus the strain and degree of saturation by introducing constant gravimetric water content during the loading (Sun *et al*. 2008), which is successful due to introduction of the dry density on the soil-water characteristic.

2.5 Model parameters and their determination

The model being formulated within an elastoplastic framework, the strains consist of both elastic and plastic parts. The model requires five parameters to describe the stress-strain behaviour ($\lambda(0)$, λ_{s}, κ, p'_{n} and M) and three parameters to describe the water-retention behaviour (λ_{sr}, κ_{s} and λ_{sc}). Two tests are required to determine the model parameters. First, an isotropic compression test is conducted on unsaturated soil under a constant suction. Secondly, an unsaturated soil specimen is loaded to a low net stress (for example, p = 50 kPa), and is then wetted to a saturated state. An isotropic compression test (with a loading-unloading-reloading cycle and a subsequent triaxial compression test) is then conducted on this saturated specimen. From the result of triaxial test on the saturated specimen, the internal friction angle (ϕ or M) can be determined. From the result of the isotropic compression test on the saturated specimen with a loading-unloading-reloading stress path, $\lambda(0)$ and κ can be determined. The quantity p'_{n} can be determined from the coordinates of the point where the two isotropic compression lines for the saturated and unsaturated specimens intersect. λ_{s} can be determined using Eq. (6).

The model parameters λ_{sr}, κ_s and λ_{se} define the SWCC. λ_{se} is the slope of the *e*-S_r line under constant suction, and can be determined by plotting *e* against S_r for an isotropic compression test on unsaturated soil under a constant suction. Thereafter, κ_s and λ_{sr} are determined from the results of a wetting test at a low net stress using Eqs (2) and (3).

The elastic component is calculated from Hooke's law, with Poisson's ratio assumed to be 1/3. The elastic modulus is calculated as for the Cam-clay model:

$$E = \frac{p'(1+e)}{\kappa} \tag{19}$$

The values of the relevant model parameters used in predicting the hydro-mechanical behaviour of Pearl clay are as follows:

$$\lambda(0) = 0.12, \kappa = 0.03, \lambda_s = 0.12, p_n^{'} = 2MPa, M = 1.1, \lambda_{se} = 0.35,$$
$$\lambda_{sr} = 0.13, \kappa_s = 0.01$$

Details of the Pearl clay properties, specimen preparation, triaxial apparatus, and testing procedure can be found in Sun *et al.* (2007d).

2.6 Model simulations

The stress paths in simulations of the test results were specified in terms of net stress ($\sigma_{ij} - u_a\delta_{ij}$) and suction *s*. Increments in σ'_{ij} are given by differentiating Eq. (4) according to

$$d\sigma'_{ij} = d(\sigma_{ij} - u_a\delta_{ij}) + (S_r ds + s dS_r)\delta_{ij} \tag{20}$$

Substituting Eqs (2) and (3) into Eq. (20) gives:

$$d\sigma'_{ij} = d(\sigma_{ij} - u_a\delta_{ij}) + ((S_r - \kappa_s)ds - \lambda_{se} s de)\delta_{ij} \tag{21}$$

$$d\sigma'_{ij} = d(\sigma_{ij} - u_a\delta_{ij}) + ((S_r - \lambda_{sr})ds - \lambda_{se} s de)\delta_{ij} \tag{22}$$

Because both Eq. (21) and Eq. (22) involve d*e*, they must be solved simultaneously with a constitutive model equation before the stress path can be defined in terms of the stress-state variables (the 'average skeleton stress' tensor σ'_{ij} and the suction *s*).

Figure 7 shows comparisons between the predicted and measured results of an isotropic compression test under constant suction of 147 kPa and subsequently a wetting test by decreasing the suction from 147 kPa to zero on unsaturated compacted Pearl clay. In addition to the above-mentioned model parameters, the initial state is needed in the model predictions: p_0 = 20 kPa, s_0 = 140 kPa, e_0 =1.35, and p_{0y} =15 kPa. It can be seen that the model provides good predictions of the stress-strain relationship and the change in degree of saturation.

Figure 8 shows a comparison of the predicted and measured results of triaxial compression tests on unsaturated Pearl clay under constant mean net stress (p = 196 kPa) and constant suction (s =147 kPa). It can be seen that the model not only predicts the stress-strain relationship well, but also predicts well the change in the degree of saturation even under constant suction of 147 kPa, as shown in Figure 8(b). The traditional constitutive model such as BBM or uncoupled constitutive model for unsaturated soils cannot predict the change in the degree of saturation during loading under constant suction

Figure 9 shows a comparison of the predicted and measured results of triaxial compression tests on unsaturated compacted Pearl clay under constant mean net or effective stress (p = 196 kPa), in which a wetting path (s = 147 kPa→0 kPa) was imposed with a stress ratio (σ_1/σ_3) of about 2.0 during shear. The model predicts the stress-strain behaviour and the soil-water characteristic under complex loading path including constant suction, suction decrease and zero suction.

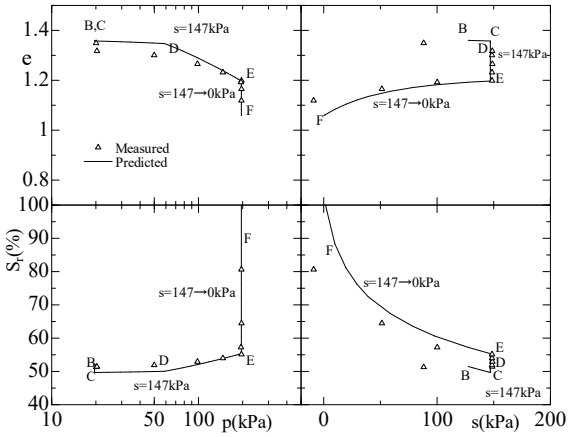

Figure 7 Predicted and measured results of isotropic compression test with *s*=147 kPa and wetting test with *s* = 147→0 kPa (after Sun *et al*. 2007c)

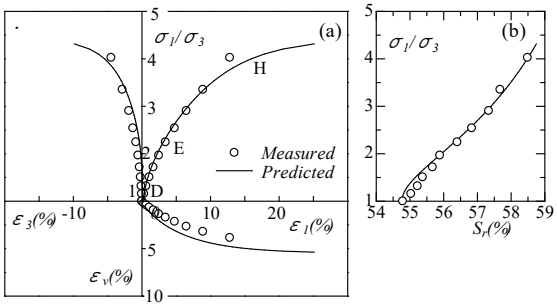

Figure 8 Predicted and measured results of triaxial compression test under p = 196 kPa) and s = 147 kPa (after Sun *et al*. 2007c)

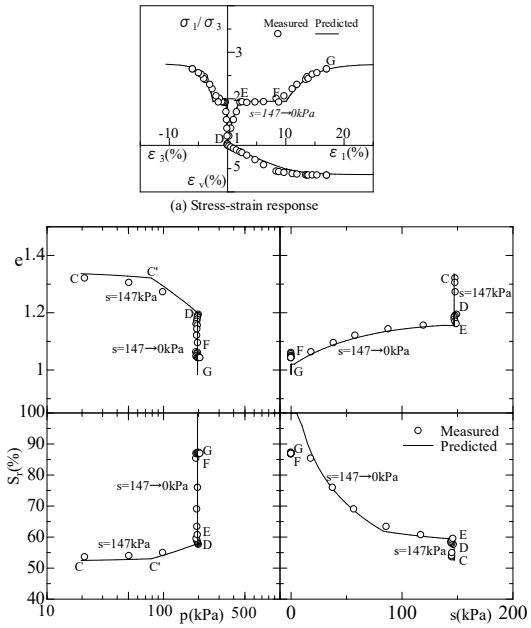

Figure 9 Predicted and measured results of triaxial compression test under s = 147 kPa, wetting (s = 147→0 kPa) and zero suction and p = 196 kPa (after Sun *et al*. 2007a)

From Figures 7, 8 and 9 it can be seen that the model provides a satisfactory description of the stress-strain relation and water-retention behavior of unsaturated clay. Indeed, the model can provide a good prediction of the stress-strain-volume-change behaviour and the soil-water characteristic of unsaturated compacted soil during the processes of constant suction (CDE in Figure 7, DEH in Figure 8, CC'DE in Figure 9), during suction reduction (EF in Figures 7 and 9), and at zero suction (FG in Figure 9) under isotropic stress or triaxial compression stress.

Figure 10 shows the measured and predicted results of the isotropic compression test on unsaturated compacted Pearl clay with the initial suction of 118 kPa, under undrained conditions, in terms of the relations: (a) void ratio versus mean net stress, (b) void ratio versus suction, (c) degree of saturation versus mean net stress, and (d) degree of saturation versus suction, i.e., soil-water characteristic curve. The isotropic net stress was applied from 20 kPa to 600 kPa under undrained conditions, with the pore-water pressure being measured and the pore-air pressure being kept at atmospheric pressure during isotropic loading. The hydro-mechanical behaviour of unsaturated soils under undrained condition was predicted using the identical parameters as the above.

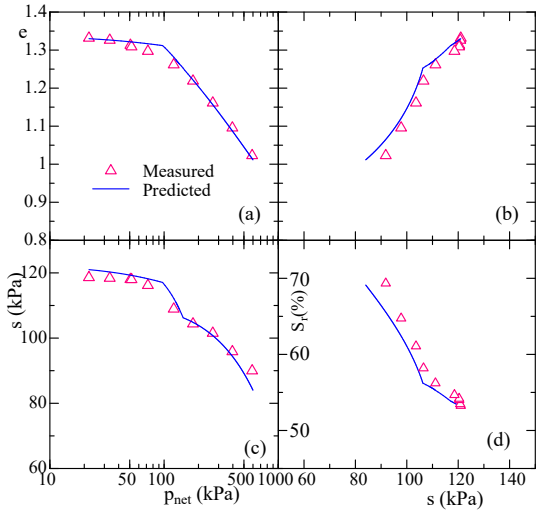

Figure 10 Measured and predicted results of isotropic compression test on unsaturated Pearl clay under undrained condition (after Sun *et al*. 2008)

Figure 11 shows predicted and measured results for an undrained triaxial compression test on unsaturated compacted Pearl clay. During the triaxial shear test, the net lateral pressure was kept constant at 100 kPa. In order to measure the suction correctly, the axis-translation technique was adopted in the test, i.e., a constant pore air pressure of 100 kPa was applied to the specimen. As a result a positive pore water pressure u_w was observed during shearing. Initial values of s_0 = 64.0 kPa, e_0 = 1.2, S_{r0} = 70.1% and p_{0y} = 20 kPa were observed at the beginning of triaxial shear test, and these values were used as the initial values in the model predictions. From the comparison, it is interesting to note that the model provides not only a good prediction of the stress–strain behaviour, but also the suction and degree of saturation response. Both the measurement and prediction show that the suction decreases and the degree of saturation increases during triaxial compression, with the net confining pressure being kept constant under undrained conditions.

As well known, the soils have hysteretic soil-water characteristics in the wetting and drying cycle, as shown in Figure 12, where the water-retention states of two compacted Pearl clay specimens (Test 1 and Test 2) are shown. The initial states (including water content, dry density and suction) of the two specimens are the same. When the specimen in Test 2 experienced the wetting and drying process from the initial state A to point C, the degree of saturation change is large even under the same suction of 100 kPa. Are the mechanical and hydraulic behaviour of two specimens with and without experiencing the wetting and drying the same?

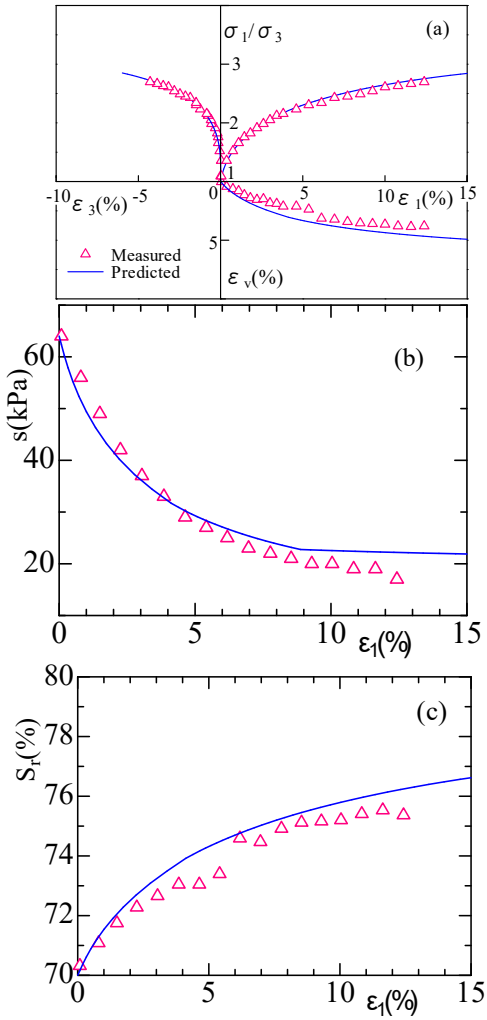

Figure 11 Measured and predicted (a) stress–strain, (b) suction versus axial strain and (c) degree of saturation versus axial strain relationships from undrained triaxial compression test at constant net confining stress of 100 kPa (after Sun *et al*. 2008)

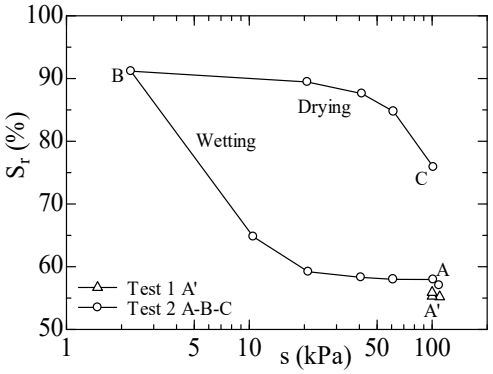

Figure 12 Suction paths for Test 1 and Test 2

The plots in Figure 13 are measured stress-strain relationship and the change in suction in triaxial shearing. It can be seen that even along the same stress/suction path for triaxial shearing, the stress-strain relationship and the change in suction are different for the two specimens (Test 1 and Test 2) with different initial degrees of saturation. The coupled hydraulic and mechanical elastoplastic model with the 'average skeleton stress' and suction being used as the stress constitutive variables can capture the differences, as shown in Figure 13. However, if the net stress and suction are used as the stress constitutive variables like the BBM, the differences in the stress-strain relationship and the change in suction between Test 1 and Test 2 cannot be captured. This is because the 'average skeleton stress' used in the coupled model takes the degree of saturation into consideration.

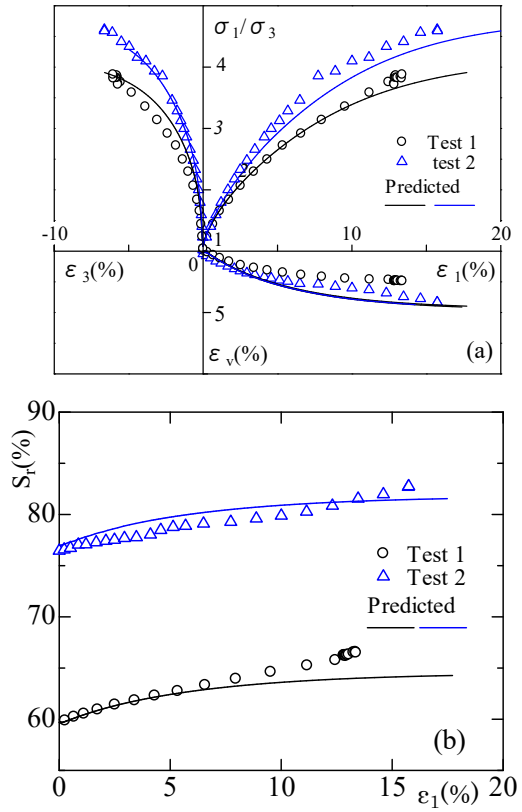

Figure 13 Predicted and measured results of triaxial compression tests for different initial degrees of saturation under p = 200 kPa and s = 100 kPa (after Sun *et al*. 2010)

3. HYDRO-MECHANICAL MODEL FOR EXPANSIVE SOILS

The above model is applicable to non-expansive unsaturated soils, and it cannot describe the swelling characteristics in wetting. In this section, an elastoplastic constitutive model is presented from the macroscopic observation for predicting the hydraulic and mechanical behaviour of unsaturated expansive soils, by modifying the above model (Sun *et al*. 2007c).

3.1 Soil-water characteristic

The SWCCs of unsaturated expansive soils at different void ratios are assumed in Figure 5, which are the same as those of non-expansive unsaturated soils.

3.2 Stress-state variables

The stress-state variables employed are the same as those in the hydro-mechanical model for non-expansive soils.

3.3 Initial yield curve (IYC)

Figure 1 is the sketch of compression curves of expansive soils. $\lambda(0)$, $\lambda(s_1)$ and $\lambda(s_2)$ are the slopes of normal compression lines of saturated soil and unsaturated soils with suctions s_1 and s_2, respectively, p_{0y}, p'_{1y} and p'_{2y} are the initial yield stresses for saturated soil and unsaturated soils with suctions s_1 and s_2. It can be seen from Figure 14 that the initial yield stress increases with increasing suction, which has the same tendency as the LC curve in the BBM. However, the compression curve is located down with increasing suction, which is different from the BBM.

The specimens with the same initial state are wetted or dried to different target suctions and then are compressed under different constant suctions. The initial yield stress will change with the imposed suction, and the initial yield curve (IYC) is a curve in the s-p' plane, which expresses the change in the initial yield stress with the suction. IYC can be defined by

$$\frac{p'_y}{p'_n}=\left(\frac{p_{0y}}{p'_n}\right)^{\frac{\lambda(0)-\kappa}{\lambda(0)[(1+r)e^{\alpha\cdot s}-r]-\kappa}} \tag{23}$$

where p'_y is the initial yield stress for unsaturated expansive soil with suction s; p'_n is an isotropic stress at which no swelling or collapse occurs when suction is decreased; r and α are the material parameters.

The IYC is used to judge whether the soil reaches the yielding state. When the stress state is inside the IYC, the specimen is at the elastic state; when the stress state reaches the IYC, the elastoplastic deformation takes place and can be obtained by using the concept of the Equivalent Void Ratio Curve (EVRC) in the next section.

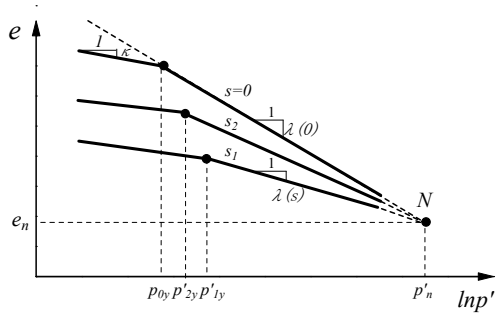

Figure 14 Sketch of compression curves of expansive soils

3.4 Equivalent void ratio curve (EVRC)

In Figure 15(a), a horizontal dash-dotted line crosses the compression curves at different suctions in the elastoplastic stage. On the line, the plastic void ratios at different suctions are the same. It can be seen that the average skeleton stress increases with decreasing suction. In order to describe this trend, the concept of equivalent void ratio curve (EVRC) is introduced when the stress state is inside the IYC, the EVRC is the line paralleled to p' axis at suction s; when the stress state reaches the IYC, the EVRC can be defined by

$$p'_y=p'_n\left(\frac{p_{0y}}{p'_n}\right)^{\frac{\lambda(0)-\kappa}{\lambda(s)-\kappa}} \tag{24}$$

$$\lambda(s)=\lambda(0)\cdot[(1-\xi)\cdot e^{(-\tau)\cdot s}+\xi] \tag{25}$$

where ξ and τ are the material parameters for identifying the change of $\lambda(s)$ with suction s.

3.5 Coupled model for isotropic stress state

A simple constitutive model for isotropic stress states is presented here. Differentiating Eq. (4) gives the increment of the 'average skeleton stress'

$$dp' = dp + S_r ds + s dS_r \tag{26}$$

where p and p' are the isotropic net stress and average skeleton stress. Substituting Eq. (2) into Eq. (26) gives

$$dp' = dp + S_r ds + s(-\lambda_{se} de - \beta \frac{ds}{s}) \tag{27}$$

where de is the elastic deformation under constant suction, that is

$$de = -\frac{\kappa \cdot dp'}{p'} \tag{28}$$

Substituting Eq. (28) into Eq. (27) and arranging gives

$$dp' = \frac{dp + (S_r - \beta) ds}{p' - \lambda_{se} \kappa s} p' \tag{29}$$

When the initial 'average skeleton stress' $p' = p_{net} + s_1 S_r$ with suction s_1 is less than the corresponding initial yield stress p'_{1y}, the strain increment consists of the elastic strain increment caused by the change of the 'average skeleton stress' (p': $p'_1 \rightarrow p'_2$) and the plastic strain increment caused by the change of suction (s: $s_1 \rightarrow s_2$), as shown in Figure 15. When the initial 'average skeleton stress' $p' = p_{net} + s_1 S_r$ with suction s_1 is greater than the initial yield stress p'_{1y}, the strain increment consists of the elastic strain increment caused by the change of the 'average skeleton stress' (p': $p'_3 \rightarrow p'_4$) and the plastic strain increment caused by the change of suction (s: $s_1 \rightarrow s_2$). In Figure 15, the suction decreases from s_1 to s_2, the swelling deformation can be predicted no matter the initial state is elastic or plastic one.

The elastic volumetric strain increment caused by p' is given by Eq. (10). The plastic volumetric strain increment caused by s is given by

$$\begin{aligned} de^p &= e^p(s_2) - e^p(s_1) \\ &= (\kappa - \lambda(s_2)) \cdot \ln \frac{p'_y(s_2)}{p'_n} - (\kappa - \lambda(s_1)) \cdot \ln \frac{p'_y(s_1)}{p'_n} \end{aligned} \tag{30}$$

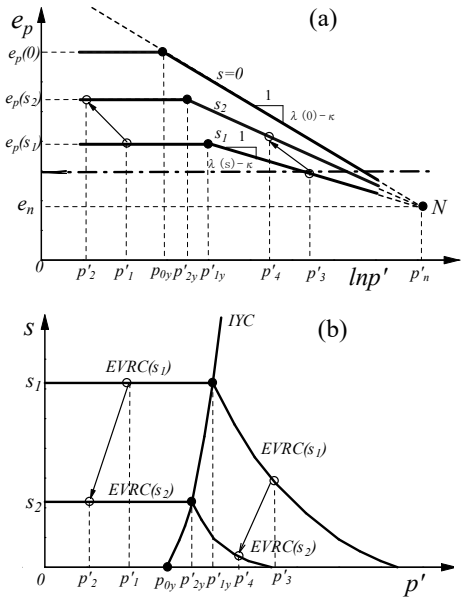

Figure 15 Sketch of the model for isotropic stress state

Given the increment of the net stress and suction, the volumetric strain increment can be calculated by Eqs. (28), (29) and (30), and the increment in the degree of saturation S_r can be calculated by

$$dS_r = (dp' - dp - S_r ds)/s \tag{31}$$

After the initial state reaches IYC as shown in Figure 15, the plastic strain increment caused by the changes in 'average skeleton stress' (p': $p'_3 \rightarrow p'_4$) and suction (s: $s_1 \rightarrow s_2$) is described by Eq. (11).

From Eq. (23),

$$dp'_y = \frac{\partial p'_y}{\partial p_{0y}} dp_{0y} + \frac{\partial p'_y}{\partial s} ds \tag{32}$$

During the elastoplastic deformation stage the increments in p'_y is given by differentiating Eq. (4) according to

$$dp'_y = dp_y + S_r ds + s dS_r \tag{33}$$

where p_y is an isotropic net stress in the elastoplastic range. Substituting Eqs. (2), (10) and (32) into Eq. (33) and arranging gives

$$dp'_y = \frac{dp_y + B ds}{(1 - A) p'_y - \lambda_{se} s \kappa} p'_y \tag{34}$$

where

$$A = \lambda_{se} s (\lambda(0) - \kappa) / (p_{0y} \frac{\partial p'_y}{\partial p_{0y}}) \tag{35}$$

$$B = S_r - \beta - A \frac{\partial p'_y}{\partial s} \tag{36}$$

Given the increment of the net stress and suction, when $dp'_y > 0$, volumetric strain increment can be calculated by Eqs. (10) and (12) with Eq. (34); when $dp'_y = 0$, volumetric strain increment can be calculated by Eqs. (10) and (30) with Eq. (29), and the increment in the degree of saturation can be calculated by

$$dS_r = (dp'_y - dp_y - S_r ds)/s \tag{37}$$

The model for the isotropic stress can be extended to general stress including triaxial stress and three-dimensional stress. See Sun and Sun (2012) for details.

3.6 Predictions versus experimental results

3.6.1 Test description

Zhan (2003) conducted a series of triaxial tests on compacted unsaturated expansive clay using a suction-controllable double-cell triaxial apparatus for unsaturated soils. The montomorillonite content of the clay is 21%, and the clay belongs to the medium expansive soil. Statically compacted specimens were used in his testing program. The initial water content is 18.5%, the initial dry density is 1.56 Mg/m^3, and the initial suction is about 540 kPa, which was measured by the high suction tensiometer (Zhan, 2003).

Five tests named RST5, RUT7, RUT8, RUT9 and RUT10 are selected to verify the proposed model. The stress path of RST5 test consists of wetting from the initial state to saturation and isotropic compression to a maximum stress of 400kPa. The other four tests (RUT7, RUT8, RUT9 and RUT10) are isotropic compression tests on unsaturated expansive clay with target suctions of 25, 50, 100 and 200 kPa, respectively. After wetting tests, the four specimens were compressed to a maximum net stress of 200 kPa, and then drained triaxial shear tests were conducted on the five specimens under constant confining net pressure of 200 kPa and suctions of 25, 50, 100 and 200 kPa.

From the changes in the water content and volume of the specimens obtained in the wetting test results (Zhan, 2003), the SWCC of unsaturated expansive clay is depicted as shown in Figure 16.

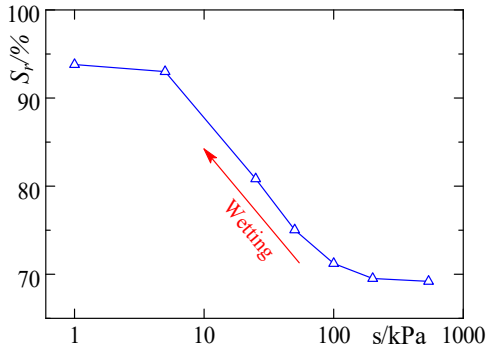

Figure 16 Measured SWCC of expansive clay

Figure 17 shows the S_r - e relation from the results of isotropic compression tests on the unsaturated expansive clay under different constant suctions. The measured S_r - e relation is linear and the gradients of the lines under different suctions are almost the same.

Based on the test data in Zhan (2003), the relevant model parameters used for predicting the stress-strain relation and soil-water characteristics of the expansive clay are determined as follows: $\lambda(0)$=0.11, κ=0.02, ξ=0.3489, τ=0.0294kPa^{-1}, p'_n=300kPa, M=0.97, γ=-1.46, α=-1.09, p'_{iy0}=60kPa, λ_{sr}=0.1, κ_s=0.03, S_{0rw}=45.1%, λ_{se} =0.83.

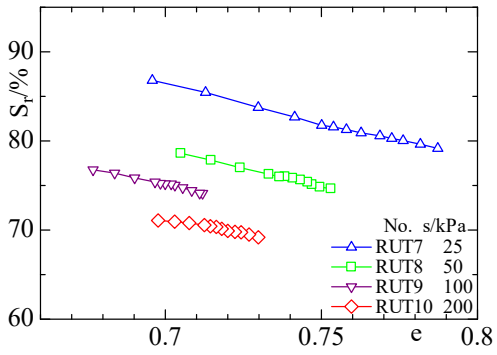

Figure 17 Relationship between degree of saturation and void ratio during compression under different constant suctions

3.6.2 Predictions on wetting tests under constant net stress

For the wetting tests under a constant isotropic net stress of 20 kPa (Figure 18), the suctions of four specimens (RUT7, RUT8, RUT9 and RUT10) were decreased from an initial suction of 540 kPa to the target suctions of 25, 50, 100 and 200 kPa, respectively. Figure 18 shows the changes in void ratio and degree of saturation before and after the wetting tests and its prediction of their changing process.

From the predicted results in Figure 18 (b), it can be seen that when the suction decreases to the values smaller than 100 kPa, the increase tendency of the saturation degree of specimens in RUT7 and RUT8 is more obvious. It can be analyzed from the SWCC in Figure 16. When the suction decreases to 100 kPa during wetting, the wetting curve changes from the scanning curve to the main wetting curve.

The comparisons indicate that the proposed coupled model provides good predictions of the changes in void ratio and degree of saturation of unsaturated expansive clay during wetting at constant net stress.

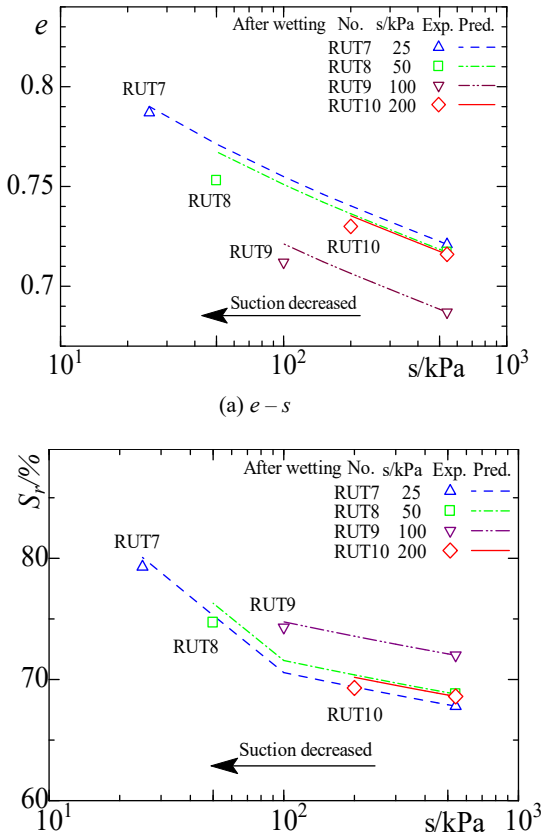

Figure 18 Changes in void ratio and degree of saturation during wetting from initial state to targeted suctions (after Sun and Sun 2012)

3.6.3 Predictions on compression tests under constant suctions

Figure 19 shows the changes in void ratio and degree of saturation of four specimens of RUT7 to RUT10 during compression under constant suctions of 25, 50, 100 and 200 kPa. From Figure 19 (a), it can be seen that the predicted results are consistent with the deformation of the specimen during compression. At the same time, the coupled model can also predict that the changing of the degree of saturation with the increase in the isotropic net stress even at constant suction (Fig. 19b), which cannot be predicted by the BExM (Alonso et al. 1999). So the coupled model can predict not only the deformation but also the soil water characteristics of unsaturated expansive clay.

3.6.4 Predictions on triaxial shear tests under constant suctions

After the isotropic compression, the drained triaxial shear tests under constant net confining pressure (σ_3=200kPa) are conducted on the five specimens RST5 and RUT7 to RUT10 under respective target suctions. Figure 20 shows the comparisons of predicted and measured results in terms of deviatoric stress (Figure 20a), volumetric strain (Figure 20b) and water content (Figure 20c) with the axial strain. From the triaxial shear test results, it can be seen that five stress-strain curves present the outer convex shape, the initial rigidity and the deviatoric stress at failure increases with increasing suction. Contractive volumetric strain can be observed in five tests. During shearing, the water content decreases for suctions of 0 and 25 kPa, and increases a little for other suctions.

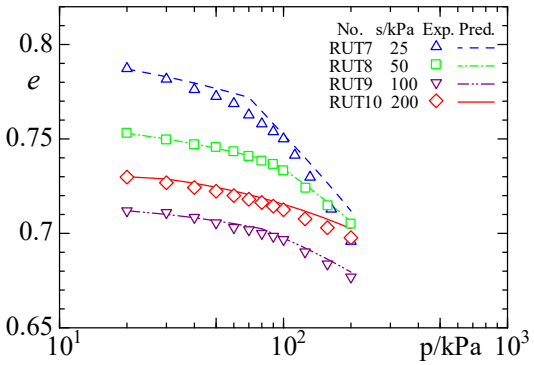

(a) $e - p$

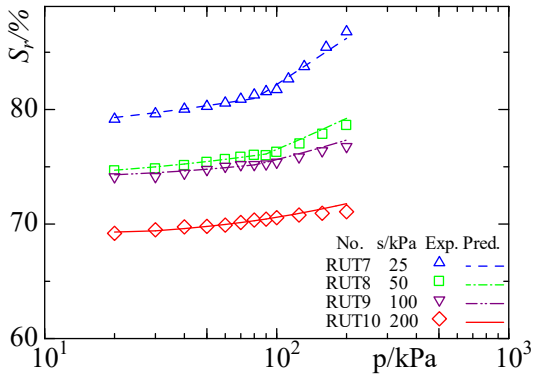

(b) $S_r - \sigma_v$

Figure 19 Changes in void ratio and degree of saturation during compression under constant suctions (after Sun and Sun 2012)

The initial average skeleton stress p' is larger than the initial yield stress p'_{iy} under the confining pressure of 200 kPa. Therefore, the specimens are kept in elastoplastic stage during the triaxial shear tests. The deformation can be calculated according to the equations of the elastoplastic stage.

It is noted that Figure 20(b) does not present the good regular relationship between volumetric strain and axial strain, especially the contractive deformation is the smallest for zero suction. It is well known that it is difficult to measure the volume change in triaxial tests on unsaturated soils. From the isotropic compression test result, it can be deduced that the contractive strains due to shearing should decrease with increasing suction, because the compression index decreases and the rigidity of the soil increases. According to the predicted results using the coupled model, volumetric strains increase with decreasing suction (Figure 20b). Also, the predicted stress-strain relations in Figure 20(a) are consistent with the test results. The coupled model provides a good description of the changes of strength and deformation. At the same time, it can also predict the changes of water content with shearing even at constant suction. Therefore the coupled model can predict not only the deformation but also the soil-water characteristics of unsaturated expansive soils.

4. CONCLUSION

Two elastoplastic constitutive models for non-expansive and expansive unsaturated soils were illustrated for isothermal conditions. It was observed that by adopting the approach with incorporation of the suction-degree of saturation relationship into the stress-suction-strain relationship, the two coupled constitutive model can satisfactorily describe the hydro-mechanical behavior of unsaturated soils.

There are a few limitations in the proposed models for describing the unsaturated soil behaviour. For example, the model ignored the existence of minimum void ratio where suction can no longer reduce the void ratio of soil below this suction value.

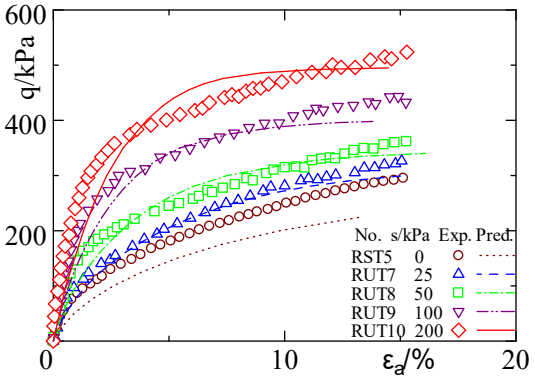

(a) q - ε_a

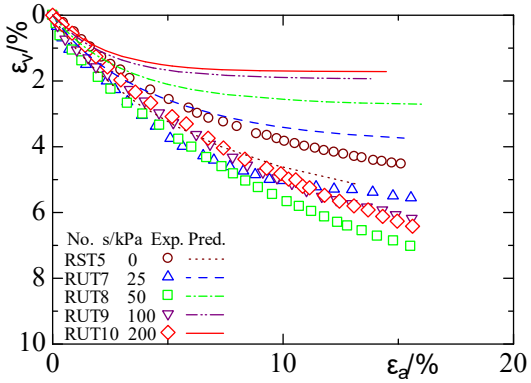

(b) ε_v - ε_a

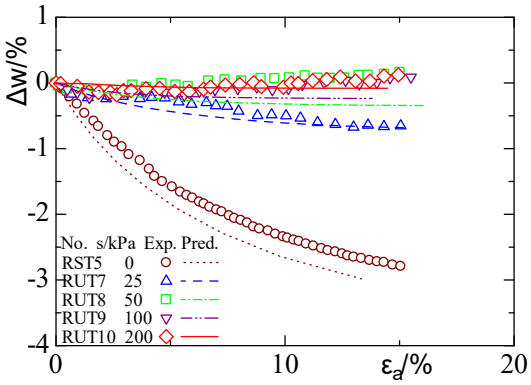

(c) Δw - ε_a

Figure 20 Test results and predictions of triaxial shear tests under constant suctions (σ_3=200kPa)

5. ACKNOWLEDGEMENTS

The authors express their gratitude for the grants provided by the National Natural Science Foundation of China (Nos. 41602295 and 11672172).

6. REFERENCES

Alonso, E. E., Gens, A. and Hight, D.W. (1987). "Special problem soils." General report. Comptes Rendus de la 9ème Conference Européenne de Mécanique des Sols et des Travaux de Fondations, 3:1087-1146, Dublin.

Alonso, E. E., Gens, A. and Josa, A. (1990). "A constitutive model for partially saturated soils." Géotechnique, 40(3): 405-430.

Alonso, E. E., Vaunat, J. and Gens, A. (1999). Modelling the mechanical behaviour of expansive clays. Engineering Geology, 54 (1): 173 – 183.

Bishop, A. W. and Blight, G. E. (1963). "Some aspects of effective stress in saturated and partly saturated soils." Géotechnique, 13(3): 177-197.

Colman, J. D. (1962). "Stress strain relations for partly saturated soil. " Correspondence, Géotechnique, 12(4): 348-350.

Gens, A. and Alonso, E. E. (1992). "A framework for the behaviour of unsaturated expansive clays." Canadian Geotechnical Journal, 29 (6): 1013-1032.

Fredlund, D.G. and Morgenstern, N.R. (1977). "Stress state variable for unsaturated soils." Journal of Geotechnical Engineering, ASCE, 103(5): 447-466.

Gens, A. and Alonso, E.E. 1992. "A framework for the behaviour of unsaturated clay." Canadian Geotechnical Journal, 29: 1013-1032.

Gens, A., Sanchez, M. and Sheng, D.C. (2006). "On constitutive modelling of unsaturated soils." Acta Geotechnica, 1: 137-147.

Kohgo, Y., Nakano, M., and Miyazaki, T. (1993). "Theoretical aspects of constitutive modelling for unsaturated soils." Soils and Foundations, 33(4): 49-63.

Nuth, M. & Laloui, L. (2008). "Advances in modelling hysteretic water retention curve in deformable soils." Computers and Geotechnics 35(6):835-844.

Salager, S., El Youssoufi, M. S. & Saix, C. (2010). "Definition and experimental determination of a soil-water retention surface." Canadian Geotechnical Journal 47(6):609-622.

Sheng, D.C., Sloan, S.W. and Gens, A. (2004). "A constitutive model for unsaturated soils: thermomechanical and computational aspects." Computational mechanics, 33(6):453-465.

Sheng, D.C., Fredlund, D. G. and Gens, A. (2008). "A new modelling approach for unsaturated soils using independent stress variables." Canadian Geotechnical Journal, 45: 511-534.

Sun, D. A., Cui, H. B., Matsuoka, H. and Sheng, D. C. (2007a). A three-dimensional elastoplastic model for unsaturated compacted soil with hysteresis, Soils and Foundations, 47(2): 253-264.

Sun, D. A., Matsuoka, H., Yao, Y. P. and Ichihara, W. (2000). An elasto-plastic model for unsaturated soil in three-dimensional stresses, Soils and Foundations, 40(3): 17-28.

Sun, D. A., Sheng, D. C., Cui, H. B. and Sloan, S. W. (2007b). A density dependent elastoplastic hydro-mechanical model for unsaturated compacted soil, International Journal for Numerical and Analytical Method in Geomechanics, 31(11): 1257-1279.

Sun, D. A., Sheng, D. C. and Sloan, S. W. (2007c). Elastoplastic modelling of hydraulic and stress-strain behaviour of unsaturated compacted soils, Mechanics of Materials, 39(3): 212-221.

Sun, D. A., Sheng, D. C., Xiang, L. and Sloan, S. W. (2008). Elastoplastic prediction of hydro-mechanical behaviour of unsaturated soils under undrained conditions, Computers and Geotechnics, 35(6): 845-852.

Sun, D. A., Sheng, D. C. and Xu, Y. F. (2007d). Collapse behaviour of unsaturated compacted soils with different initial densities, Canadian Geotechnical Journal, 44(6): 673-686.

Sun, D. A., Sun, W. J., and Xiang, L. (2010). "Effect of degree of saturation on mechanical behaviour of unsaturated soils and its elastoplastic simulation." Computers and Geotechnics, 37(5): 678-688.

Sun, W. J., and Sun, D. A. (2012). "Coupled modelling of hydro-mechanical behaviour of unsaturated compacted expansive soils." International Journal for Numerical and Analytical Methods in Geomechanics, 36(8): 1002-1022.

Wheeler, S. J. and Sivakumar, V. (1995). "An elasto-plastic critical state framework for unsaturated soil." Géotechnique, 45(1): 35-53.

Wheeler, S. J., Sharma, R. S. and Buisson, M. S. R. (2003). "Coupling of hydraulic hysteresis and stress-strain behaviour in unsaturated soils." Géotechnique, 53 (1): 41-54.

Zhan, L. T. (2003). Field and laboratory study of an unsaturated expansive soil associated with rain-induced slope instability, Ph.D. Dissertation, Hong Kong University of Science and Technology: 302-354.